JACC: CARDIOVASCULAR IMAGING VOL. 12, NO. 3, 2019
© 2019 BY THE AMERICAN COLLEGE OF CARDIOLOGY FOUNDATION
PUBLISHED BY ELSEVIER

REVIEW

STATE-OF-THE-ART PAPER

Multimodality Imaging of the Tricuspid Valve and Right Heart Anatomy

Omar K. Khalique, MD,[a] João L. Cavalcante, MD,[b] Dipan Shah, MD,[c] Andrada C. Guta, MD,[d,e] Yang Zhan, MD,[c] Nicolo Piazza, MD, PhD,[f] Denisa Muraru, MD, PhD[e,g]

SUMMARY

The characterization of tricuspid valve and right-heart anatomy has been gaining significant interest in the setting of new percutaneous transcatheter interventions for tricuspid regurgitation. Multimodality cardiac imaging provides a wealth of information about the anatomy and function of the tricuspid valve apparatus, right ventricle, and right atrium, which is pivotal for diagnosis and prognosis and for planning of percutaneous interventions. The present review describes the role of echocardiography, cardiac magnetic resonance, and multidetector row cardiac computed tomography for right heart and tricuspid valve assessment. (J Am Coll Cardiol Img 2019;12:516–31) © 2019 by the American College of Cardiology Foundation.

The impact of right-heart (RH) disease is a subject of increasing interest. It has been shown that isolated tricuspid regurgitation (TR) is prognostically significant (1). TR status also negatively predicts prognosis in the setting of post-surgical (2,3) and post-transcatheter procedures for the aortic and mitral valves (4,5). Because the importance of treating tricuspid pathology is increasingly recognized, identification of tricuspid valve (TV) and RH pathology and anatomical planning for percutaneous interventions will become crucial. Multimodality cardiac imaging is the linchpin of TV and RH assessment. This paper describes the role of multimodality imaging including echocardiography, cardiac magnetic resonance (CMR), multidetector row computed tomography (MDCT), and fluoroscopy in the evaluation of TV and RH anatomy (**Central Illustration**).

BRIEF OVERVIEW OF NORMAL RH ANATOMY

The TV apparatus includes the 3 leaflets, the annulus, and the subvalvular apparatus (chordae tendineae, papillary muscles), and is closely linked with the right atrium (RA) and the right ventricle (RV) in the so-called "valve-ventricular complex" (6). The TV is the largest among the 4 cardiac valves. In relation to the mitral valve (MV), the TV is located more apically (≤10 mm), anteriorly, and to the right (**Figure 1**). The tricuspid leaflets are thinner than the mitral leaflets and therefore are more difficult to image. The TV annular plane is oriented nearly vertically and is rotated ~45° from the sagittal plane (7). The TV usually has 3 leaflets assigned anatomically as the septal, anterior, and posterior which close in a trifoliate fashion (**Figures 1A and 1B**). The tricuspid annulus (TA) is a complex, saddle-shaped, dynamic

From the [a]Department of Medicine, Division of Cardiology, Structural Heart and Valve Center, Columbia University Medical Center, New York, New York; [b]Minneapolis Heart Institute, Abbott Northwestern Hospital, Minneapolis, Minnesota; [c]Division of Cardiology, Houston Methodist Hospital, Houston, Texas; [d]Carol Davila University of Medicine and Pharmacy, Department of Cardiology, Bucharest, Romania; [e]Department of Cardiac, Thoracic, and Vascular Sciences, University of Padua, Padua, Italy; [f]McGill University Heart Centre, Division of Cardiology, Montreal, Quebec, Canada; and the [g]IRCCS, Instituto Auxologico Italiano, S. Luca Hospital, University of Milano-Bicocca, Milan, Italy. Dr. Khalique is a member of the Speakers Bureau for Edwards Lifesciences; and is a consultant for Cephea Valves and Jenavalve. Dr. Cavalcante has received research support from Medtronic; and is a consultant for Medtronic and Mitralign. Dr. Muraru is a consultant for, has received research support from, and is a member of the Speakers Bureau for GE Healthcare and TomTec Imaging. Dr. Piazza is a consultant for HighLife, Medtronic, MicroPort, and Cephea. Dr. Guta has received a research grant from the Romanian Society of Cardiology. All other authors have reported that they have no relationships relevant to the contents of this paper to disclose.

Manuscript received June 11, 2018; revised manuscript received January 8, 2019, accepted January 10, 2019.

ISSN 1936-878X/$36.00 https://doi.org/10.1016/j.jcmg.2019.01.006

structure (8). The nonplanar TA has higher points in the anteroseptal and posterolateral portions and lower points in anterolateral and posteroseptal portions (Figures 1 and 2). TA size and shape change significantly during the cardiac cycle.

RIGHT VENTRICLE. The RV is triangular in shape and crescent-shaped when viewed in cross-section. The RV chamber is divided into 3 components: inlet, apical trabecular, and outlet. The TV separates the RV inlet from the RA. The apical component of the RV has coarser trabeculations than the left ventricle (LV) apex. The RV outlet presents a "crossover" relationship with the LV outflow tract (Figure 1B). The RV roof is formed by the crista supraventricularis (or supraventricular crest) consisting of the ventriculoinfundibular fold and the trabecula septomarginalis, which contains the right bundle branch and continues as the moderator band (Figures 1B and 1E). Because of the complex shape of the RV, the 3 components are difficult to simultaneously image in a single cross-sectional view by using 2-dimensional (2D) echocardiography (2DE).

A complete anatomical overview of the RH can be found in an accompanying publication (9).

INTERVENTIONAL CONSIDERATIONS. Several structures adjacent to the TA are relevant for interventional procedures (Table 1). 1) The anteroseptal commissure is adjacent to the noncoronary sinus of Valsalva (Figures 1A and 1C); there is risk of aortic perforation with devices that require anchoring at this level. 2) The His bundle is located 3 to 5 mm posterior to the anteroseptal commissure adjacent to the TV septal leaflet attachment on the membranous septum: there is risk of heart blockage if pressure is applied to this region. 3) The right coronary artery within the right atrioventricular groove is adjacent to the anterior and posterior regions of the TV annulus along the RV free wall (separated by only 2 mm in some patients); there is risk of injury and acute ischemia with annular anchoring devices (Figure 1A).

As opposed to the LV, in which there is anatomic continuity and functional coupling between the atrioventricular and the semilunar valve, the TV is separated from the pulmonary valve by the ventriculoinfundibular fold (Figure 1B). The wide separation between the TV and pulmonary valve minimizes the risk of outflow tract obstruction during transcatheter TV procedures.

ECHOCARDIOGRAPHIC IMAGING OF THE TV AND RH

Echocardiography is the first-line imaging modality for the assessment of TV anatomy and function (10). Compared to other imaging modalities, the availability, safety, portability, lower costs, and excellent temporal resolution represent significant advantages, enabling patient evaluation wherever necessary. Three-dimensional echocardiography (3DE) allows full appreciation of the complexity of the TV and a better understanding of the distinctive features of TV anatomy and function, all of which provide a strong foundation for the planning and execution of complex interventional procedures (11).

TRANSTHORACIC ECHOCARDIOGRAPHIC IMAGING. Transthoracic echocardiography (TTE) is the preferred initial imaging technique for evaluating RH anatomy and function and should include a combination of views (RV inflow and short-axis, standard apical 4-chamber, apical RV-focused 4-chamber, subcostal 4-chamber, and short-axis) for optimal image definition and alignment of Doppler measurements.

The TV area can be measured by planimetry, and generally this is accomplished by 3DE, as 2DE does not allow obtaining routine proper short-axis views at the edges or tips of the valve leaflets. The normal TV area is 7 to 9 cm^2, and the transvalvular mean gradient is low (<2 mm Hg).

The structural integrity of the TV leaflets is the key feature that discriminates secondary (functional) from primary (organic) valve lesions and should be assessed from multiple views. Adjacent landmarks (aortic valve, septum, and coronary sinus) help to identify the leaflets on the basis of their anatomic relationships. However, due to its complex structure and anatomic variability, accurate identification of the leaflets from 2DE longitudinal planes remains challenging.

En face views of the entire TV by 3DE enable more reliable identification of the leaflets and commissures (Figure 1) and their spatial relationship with pacemaker leads, which is key for the diagnosis of pacemaker-related regurgitation (Figure 3). Excessive leaflet motion may indicate the presence of myxomatous valve disease or iatrogenic valve damage (after biopsy), whereas the presence of mobile masses attached to the leaflets suggests endocarditis. Thickening and restrictive motion of the leaflets can be caused by carcinoid syndrome or rheumatic involvement (Figure 3) (12).

In functional TR, the leaflets are structurally normal with normal or restricted leaflet motion due to

ABBREVIATIONS AND ACRONYMS

3D = 3-dimensional
CMR = cardiac magnetic resonance
LV = left ventricle
LVEF = left ventricular ejection fraction
MDCT = multidetector row computed tomography
MV = mitral valve
PH = pulmonary hypertension
RA = right atrium
RH = right heart
RV = right ventricle
RVEDVi = right ventricular end diastolic volume index
RVESVi = right ventricular end systolic volume index
TA = tricuspid annulus
TEE = transesophageal echocardiography
TR = tricuspid regurgitation
TTE = transthoracic echocardiography
TTVI = transcatheter tricuspid valve interventions
TV = tricuspid valve

CENTRAL ILLUSTRATION **Strengths of Imaging Modalities**

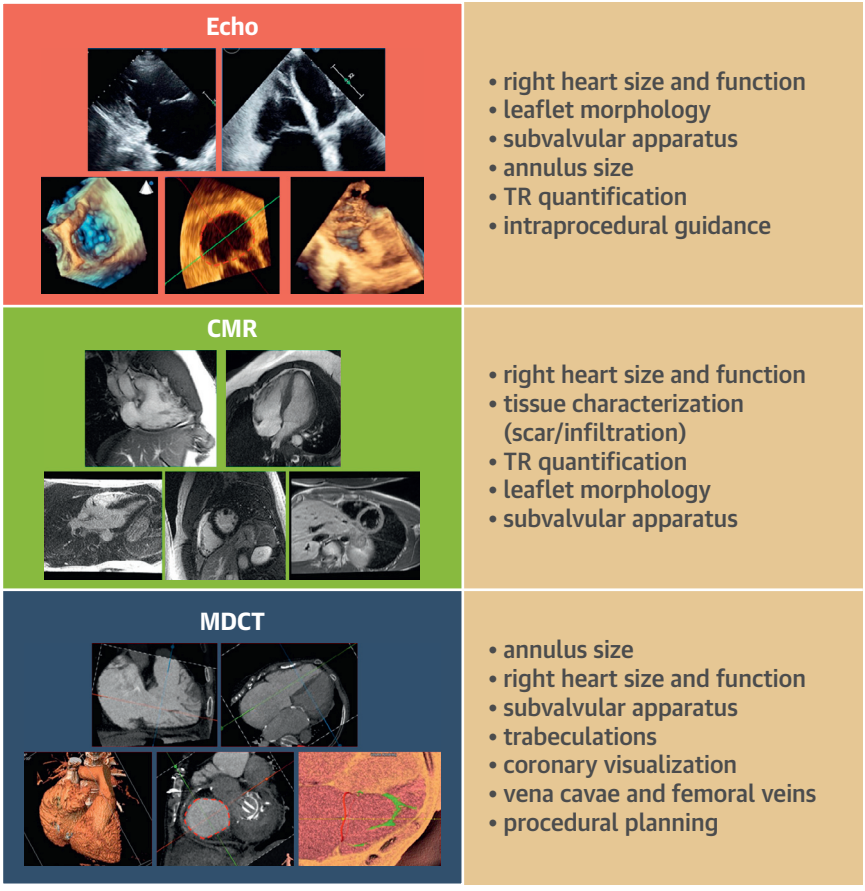

Khalique, O.K. et al. J Am Coll Cardiol Img. 2019;12(3):516–31.

CMR = cardiac magnetic resonance; Echo = echocardiography, MDCT = multidetector row computed tomography; TR = tricuspid regurgitation

RV enlargement and remodeling. From an imaging standpoint, the most relevant parameters to describe TV geometry in functional TR are annulus size and leaflet coaptation.

TA size is quantified in the apical 4-chamber RV-focused view at end diastole. Measurements performed in other views and at different times during the cardiac cycle may yield more variable results (13). The normal TA diameter in adults is 28 ± 5 mm, and significant dilation has been defined by a diastolic diameter of >40 mm or >21 mm/mm^2, although these cutoff values have been recently questioned (14). Valvular regurgitation and RH dilation are associated with a more circular, flatter, and less dynamic TA (15,16). Very large TA and lack of calcification in patients are important anatomical challenges to percutaneous interventions. It is known that 2DE underestimates the TA maximal dimension compared with 3DE, CMR, and MDCT measurements (17–19).

The mode of leaflet coaptation can be described as normal, abnormal, and absent (aka, coaptation gap). Normally, the TV leaflets coapt in a body-to-body fashion, allowing sufficient coaptation length of at least 4 mm to prevent valve incompetence. Under pathologic conditions, the TV leaflets may demonstrate reduced leaflet coaptation that can be either symmetrical (edge-to-edge), resulting in central TR, or asymmetrical (edge-to-body), resulting in eccentric TR (20). Leaflet tethering can be quantified in terms of tenting distance and tenting area at end systole (by 2DE) (**Figure 4**), and tethering/tenting volume (by 3DE). Severe, functional TR is associated with a tethering distance of >8 mm and tenting area of >1.6 cm^2 (21). Leaflet tethering is an important

FIGURE 1 **Tricuspid Valve Anatomy**

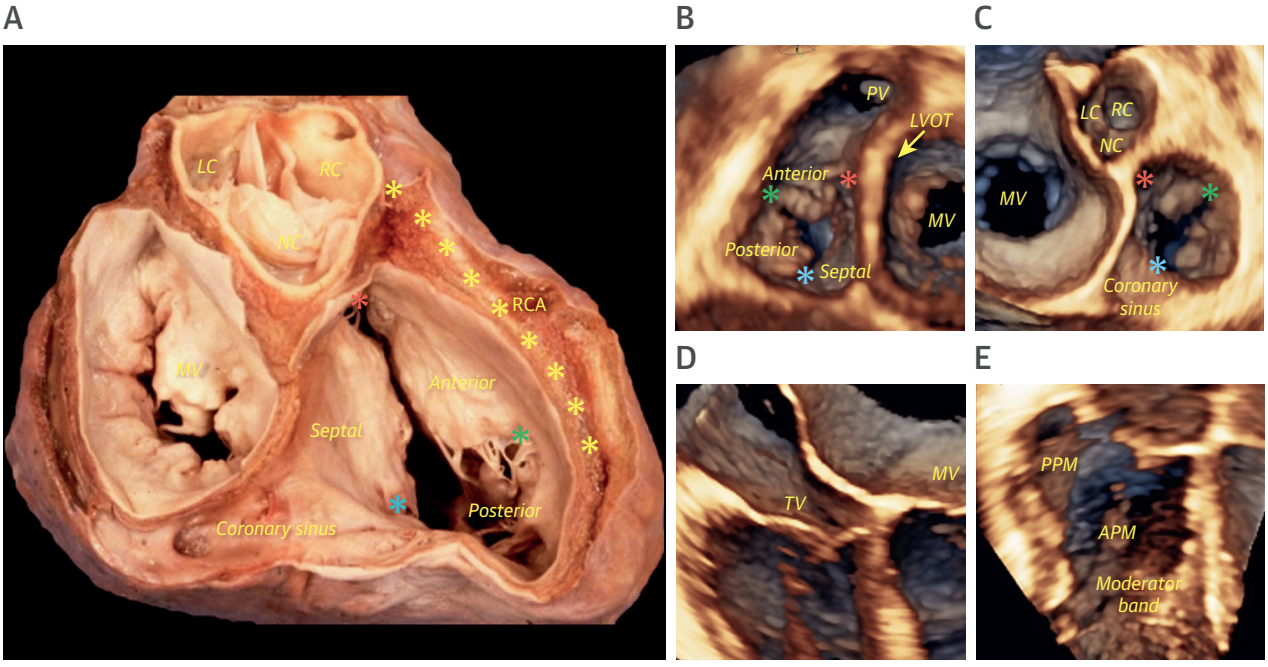

(A) Anatomical specimen with the TV anterior, septal, and posterior leaflets shown. The right coronary artery courses adjacent to the anterior portion of the tricuspid annulus in the right atrioventricular groove (courtesy of Prof. Cristina Basso, Cardiovascular Pathology, University of Padua, Italy). **(B to E)** 3D echocardiographic views of the anatomy of tricuspid valve apparatus from the ventricular aspect **(B)**, atrial aspect **(C)**, 4-chamber and papillary muscles **(D and E)**. APM = anterior papillary muscle; LC = left coronary cusp; LVOT = left ventricular outflow tract; MV = mitral valve; NC = non-coronary cusp; PPM = posterior papillary muscle; PV = pulmonary valve; RC = right coronary cusp; RCA = right coronary artery; TV = tricuspid valve; **orange asterisk** = anteroseptal commissure; **blue asterisk** = posteroseptal commissure; **green asterisk** = anteroposterior commissure.

mechanism of valve incompetence and has profound implications for the selection and outcomes of repair techniques. Consequently, the coaptation mode and leaflet tethering should be routinely evaluated and reported in patients with significant TR. One additional cause of tethering is mechanical interaction of intracardiac pacemaker or defibrillator leads with the TV apparatus.

FIGURE 2 **Tricuspid Valve Annulus Geometry and Spatial Orientation of the Commissures**

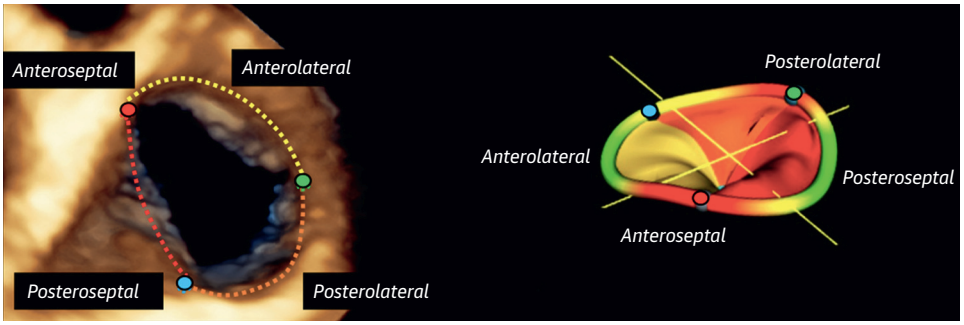

The higher (more atrial) anteroseptal and posterolateral points of the saddle-shaped tricuspid annulus are shown in **red** on the annulus 3D model reconstruction **(right)**. Lower points (more ventricular) occur at the posteroseptal and anterolateral aspects and are shown in **green**. **Yellow** = anterior leaflet; **red** = septal leaflet; **orange** = posterior leaflet; **red dot** = anteroseptal commissure; **blue dot** = posteroseptal commissure; **green dot** = anteroposterior commissure.

TABLE 1 Assessment of Tricuspid Valve and RH Anatomy and Related Interventional Considerations

General Assessment	Interventional Therapy Considerations
Right atrium	
Linear dimensions Area Maximal volume	Space to manipulate devices (MitraClip, Gate) Reached from the IVC, SVC, direct puncture
Right ventricle	
Linear dimensions Areas Volumes (end-diastolic and end-systolic) Position of papillary muscles Location and extent of trabeculations and moderator band	Clear pathway to anchor into RV apex (Forma) RVOT obstruction risk absent
Tricuspid annulus	
Linear dimensions Annular area Distance to right coronary artery at anterior aspect Width of annular shelf	Anchoring of devices onto annulus (Trialign, Gate, Cardioband) Impingement of RCA
Tricuspid leaflets	
Number of leaflets Coaptation gap(s) size and location Coaptation distance Tenting area and volume	Ability to close coaptation gap (MitraClip)
Tricuspid subvalvular apparatus	
Position of papillary muscles and distance from tricuspid leaflets Length of chordae tendinae (presence of shortening)	Navigation of devices toward RV apex (Forma)
IVC and SVC	
Linear dimensions and area Position of hepatic vein	Anchoring of devices (heterotopic Sapien implantation, TriCinch)

IVC = inferior vena cava; RCA = right coronary artery; RV = right ventricle; RVOT = right ventricular outflow tract; SVC = superior vena cava.

FIGURE 3 Tricuspid Valve Disease Processes by 3D Echocardiography

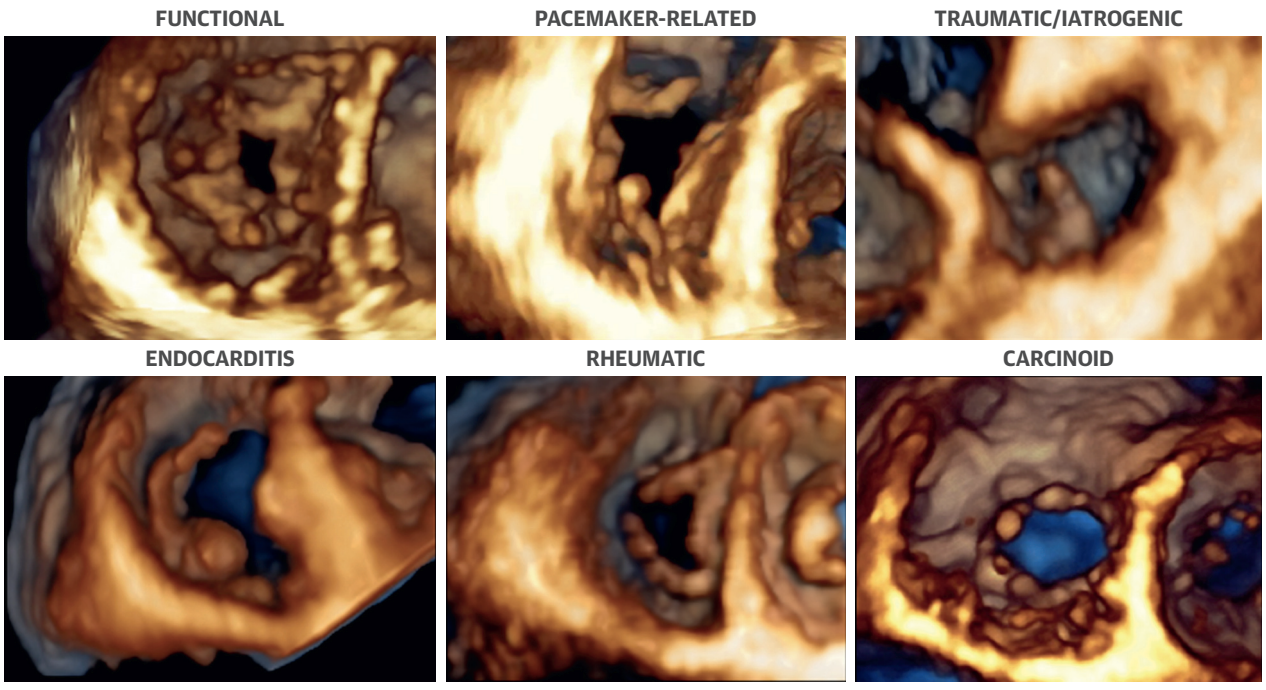

Anatomy in different tricuspid valve disease processes, illustrated by transthoracic 3-dimensional echocardiography.

FIGURE 4 Measurements of Tricuspid and Right Ventricular Geometry by Conventional 2D Echocardiography

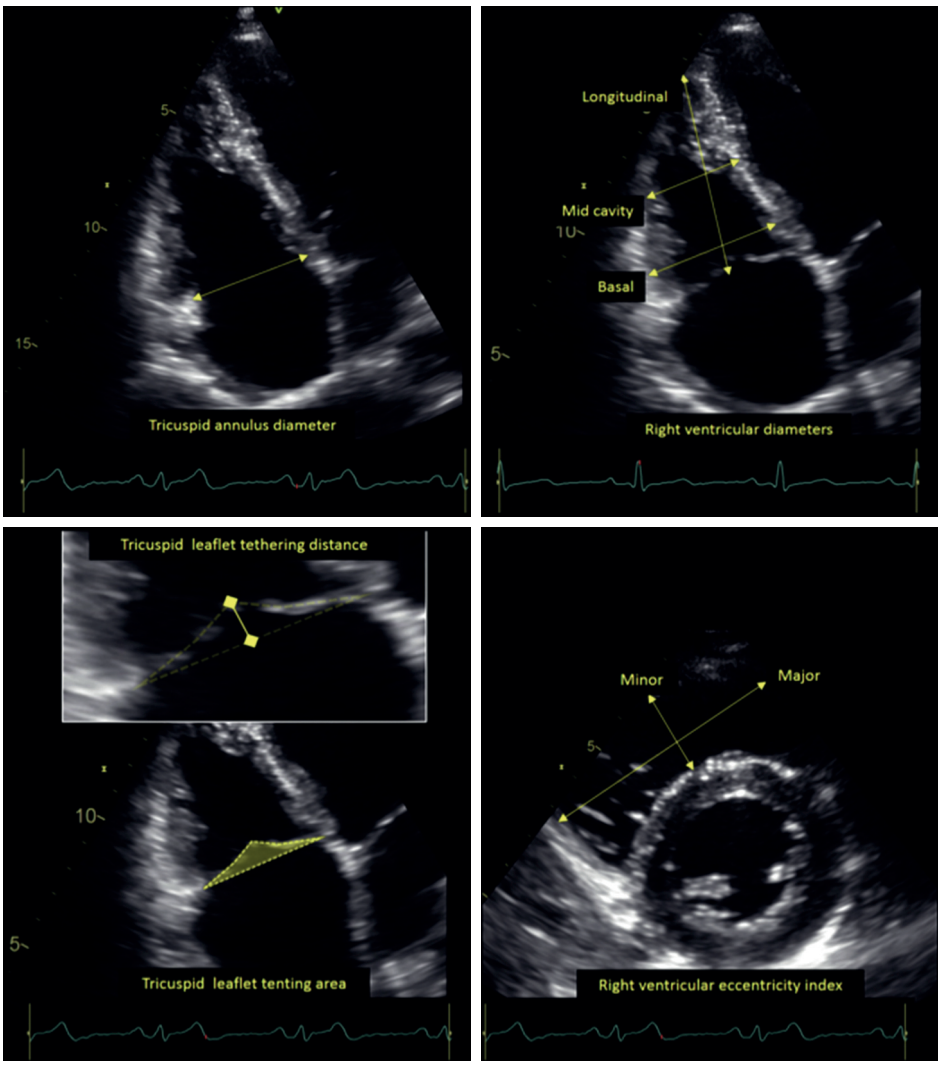

Red marker on the ECG tracings shows the timing of the measurement for each parameter. ECG = electrocardiography.

RV size can be evaluated by measuring linear dimensions and end-diastolic area from an apical RV-focused view (**Figure 4**). Proper adjustment of probe position and rotation is important to obtain a non-foreshortened, dedicated 4-chamber RV view with the largest RV transverse dimension. RV basal diameter of >41 mm, mid-cavity diameter of >35 mm, end-diastolic area of >24 cm^2 for men and >20 cm^2 for women indicate RV enlargement (22). 3DE-derived RV volume correlates well with CMR and is more accurate and reproducible than 2D RV size measurements (22,23).

Several indices of global RV shape and regional geometric remodeling can be obtained by echocardiography. RV eccentricity index can be quantified by using 2D TTE as the ratio of the major-to-minor RV diameters in the parasternal short-axis view (**Figure 4**). An increased end-systolic RV eccentricity index (>2) is an independent determinant of functional TR severity (21). RV sphericity can be quantified as the longitudinal-to-mid-cavity diameter ratio or as [(mid-cavity × longitudinal diameter])/[basal diameter]) ratio (**Figure 4**). A more spherical or elliptical shaped RV in systole may explain the severe

TABLE 2 Multimodality RH Reference Values

	Echo (82)*		CMR (32)*		CT (83)*	
	Mean ± SD	Normal Range	Mean ± SD	Range*	Mean ± SD†	95% CI
Right ventricle						
RV EDV indexed to BSA, ml/m^2	-	-	-	-	-	-
Men	61 ± 13	35–87	91 ± 15	61–121	96 ± 15	92–100
Women	53 ± 10.5	32–74	80 ± 16	48–112	88 ± 12	85–91
RV ESV indexed to BSA, ml/m^2	-	-	-	-	-	-
Men	27 ± 8.5	10–44	39 ± 10	19–59	42 ± 19	37–47
Women	22 ± 7	8–36	32 ± 10	12–52	36 ± 15	32–40
3D RV EF, %	58 ± 6.5	≥45	-	-	59 ± 15	56–62
Men	-	-	62 ± 5	52–72	58 ± 16	54–62
Women	-	-	61 ± 5	51–71	61 ± 14	51–65
Right atrium						
RA area, cm^2	-	-	22 ± 3.8	14–30	-	-
RA volume index, ml/m^2	-	-	-	-	-	-
Men	21 ± 6‡	<30 (26)*	-	-	-	-
Women	25 ± 7‡	<28 (26)*	-	-	-	-
3D RA volume index, ml/m^2	29 ± 7 (27)*	-	53 ± 16 (61)*	21–85	59.7 ± 15.0 (71)*	30.3–89.1
Men	31 ± 8	-	-	-	-	-
Women	27 ± 6	-	-	-	-	-

*References indicate sources of measurement reference values for that modality, unless specifically indicated adjacent to specific measurements. †Mean ± 2SD. ‡Simpson's single plane measurement.

BSA = body surface area; CMR = cardiac magnetic resonance; CT = computed tomography; EF = ejection fraction; RA = right atrium; RV = right ventricle.

leaflet tethering and valve regurgitation despite modest annular dilation in functional TR due to pulmonary hypertension (PH) (6). Although 3DE is more challenging for the RV than LV due to artifacts, 3DE allows for the quantification of RV regional curvature (24) without geometric assumptions, which could be useful as a metric of RV remodeling and disease progression.

RV function can be reliably measured with several echocardiographic indices. Tricuspid annular plane systolic excursion (TAPSE) toward the apex in the 4-chamber view is easy to obtain from any 2DE study. A TAPSE of <17 mm suggests RV systolic dysfunction. Tricuspid annulus systolic tissue Doppler velocity of <9.5 cm/s in the 4-chamber view suggests RV systolic dysfunction. An RV 4-chamber fractional area change of <35% indicates systolic dysfunction. RV speckle-tracking strain has shown prognostic value in a number of disease processes. 3D RV ejection fraction (RVEF) is a more global measurement of systolic performance that has been validated in a comparison with CMR (25).

The RA volume is routinely evaluated from a dedicated apical 4-chamber view by using either single-plane disk summation or the area-length method. The normal ranges for 2D RA volume indexed to body surface area are shown in **Table 2** (22,26). 3DE enables a more accurate measurement of atrial volumes without geometric assumptions (27).

TRANSESOPHAGEAL ECHOCARDIOGRAPHY. Because of the anterior position of the TV, transesophageal echocardiographic (TEE) imaging is more challenging for the TV than for the MV. When the acoustic window is satisfactory, TTE imaging of the TV may be superior in quality to TEE. If TTE windows are suboptimal, then TEE should be performed. For adequate TV imaging during interventional procedures, a combination of TEE with fluoroscopy, TTE, and intracardiac echocardiography may be necessary. If TR is suspected clinically, TEE should be performed in addition to TTE for full evaluation of TR and anatomic planning for transcatheter interventions.

Mid- and deep esophageal and transgastric views are commonly used for TEE imaging of the TV. The TA is usually measured in the mid-esophageal 4-chamber view. As with 2D TTE, 2D TEE measurements may underestimate the maximal dimension of the TV annulus. The transgastric basal short-axis view is the only 2DE view that can provide simultaneous visualization of all 3 TV leaflets. 3D TEE allows reconstruction of the TV from transgastric, mid- or deep esophageal views and visualization from the atrial and ventricular aspects.

CMR IMAGING OF THE TV AND RH

The ability to dynamically visualize the heart without body habitus limitations or need for ionizing

FIGURE 5 **Creation of RV Long-Axis Views From the Short-Axis Views**

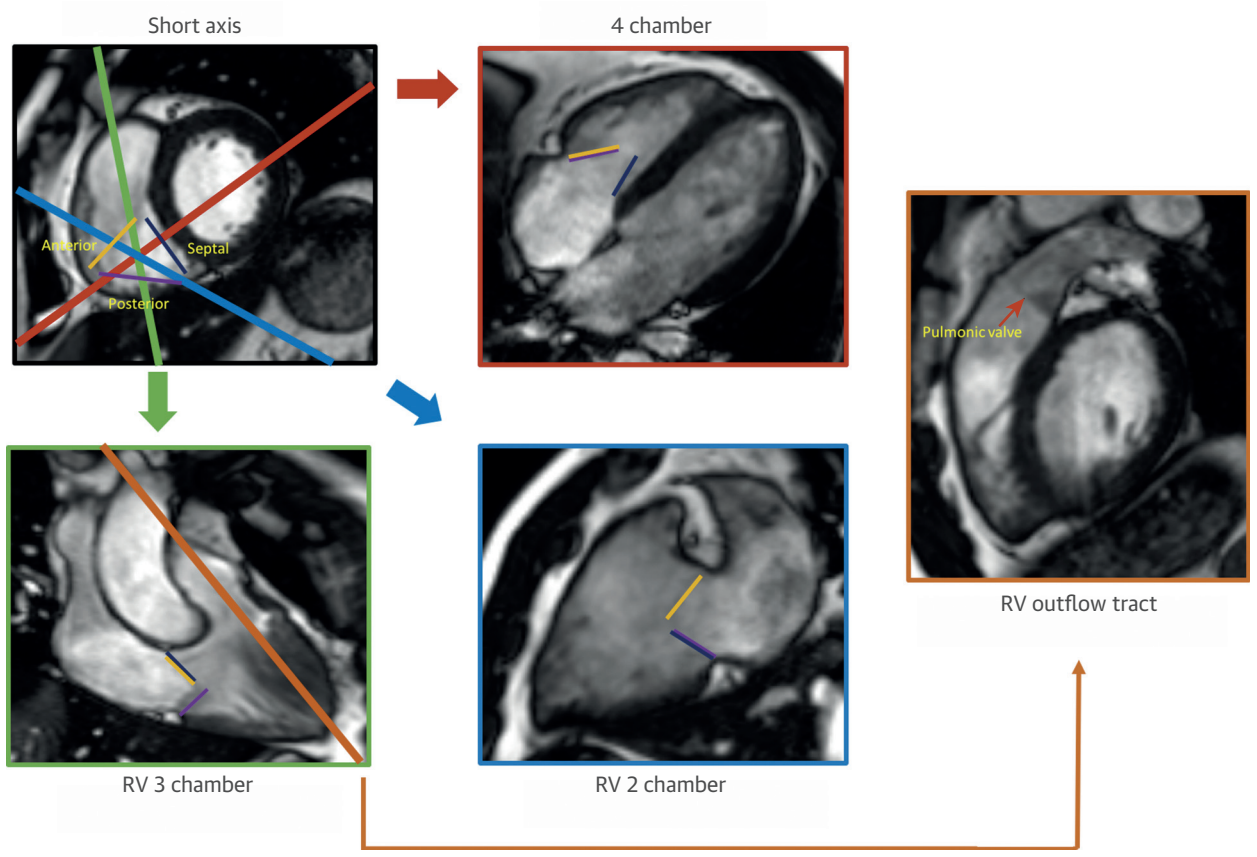

The RVOT view is created perpendicular to the RV 3-chamber view. Visualization of the tricuspid leaflets includes the septal **(blue)**, anterior **(yellow)**, and posterior **(purple)** leaflets. One of the 2 leaflets is always reliably visualized in each RV long-axis view, but the other may vary based on slice positioning. RV = right ventricular; RVOT = RV outflow tract; **Red** = 4-chamber; **green** = RV 3-chamber; **blue** = RV 2-chamber.

radiation makes CMR ideally suited to assess TV pathology and RH remodeling. RV and RA volume measurements are accurate and reproducible, and when combined with phase-contrast-derived pulmonic flow measurements, can be used to quantitate the degree of TR. Thorough evaluation of regional wall motion abnormalities and tissue characterization are uniquely possible using CMR.

RV VOLUMES AND FUNCTION. RV volumes, function, mass, and wall motion are best assessed using both short- and long-axis cine images. Balanced steady-state free-precession acquisitions yield excellent signal-to-noise ratios and high blood-to-myocardium contrast (28). A short-axis stack of images is planned from LV scout images to ensure full coverage from the base to the apex, with a slice thickness of 6 to 8 mm and a 2- to 4-mm interslice gap (29). These images will typically capture the entire RV. However, when the RV is dilated, care should be taken to ensure that the lateral subtricuspid region is included, as it may be the most basally displaced portion of the ventricle. Although the standard 4-chamber RV long-axis view is routinely acquired, specialized views are required for thorough assessment of the RV, including the RV inflow (RV 2-chamber) view, the RV inflow/outflow (RV 3-chamber) view, and the RV outflow tract (RVOT) view (Figure 5). These specialized views are planned from the stack of short-axis and acquired long-axis views. Of note, for generating the 4-chamber view, it is important to prescribe the angle from the short-axis view that reveals the largest RV dimension possible (30). Acquired cine images should achieve a temporal resolution of <45 ms per phase or >22 frames/s and can be achieved typically within a breath holding sequence of 5 to 8 s (29).

FIGURE 6 Simpson's Approach to RV Volumes With Colocalization Between Short-and Long-Axis Images, Using Post-Processing Software

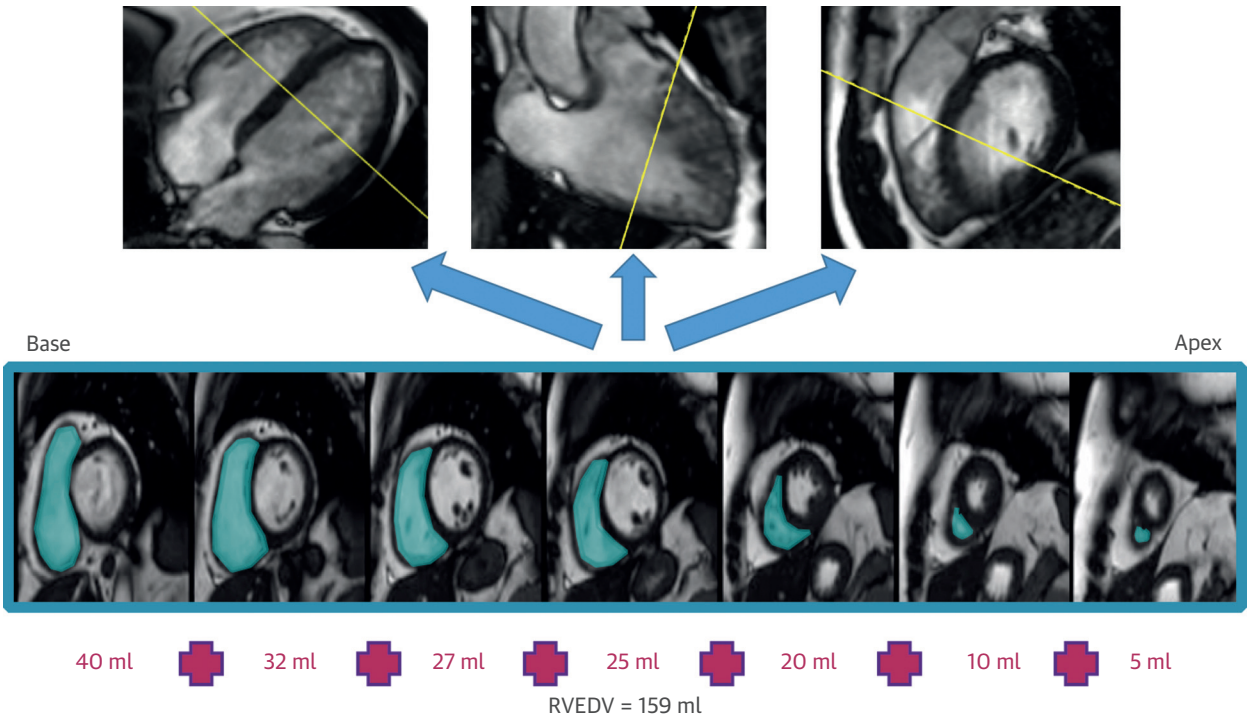

RV = right ventricular; RVEDV = right ventricular end diastolic volume.

By tracing the RV endocardial borders in each short-axis slice, volumes can be quantified using the Simpson's method of discs (Figure 6). Delineating the RV base in the short-axis orientation can be challenging; however, newer post-processing software allows colocalization of short-axis views with long-axis views to improve slice position accuracy. The end-systolic and end-diastole phases are

FIGURE 7 Pulmonic Phase Contrast Imaging to Determine Velocities and Flow

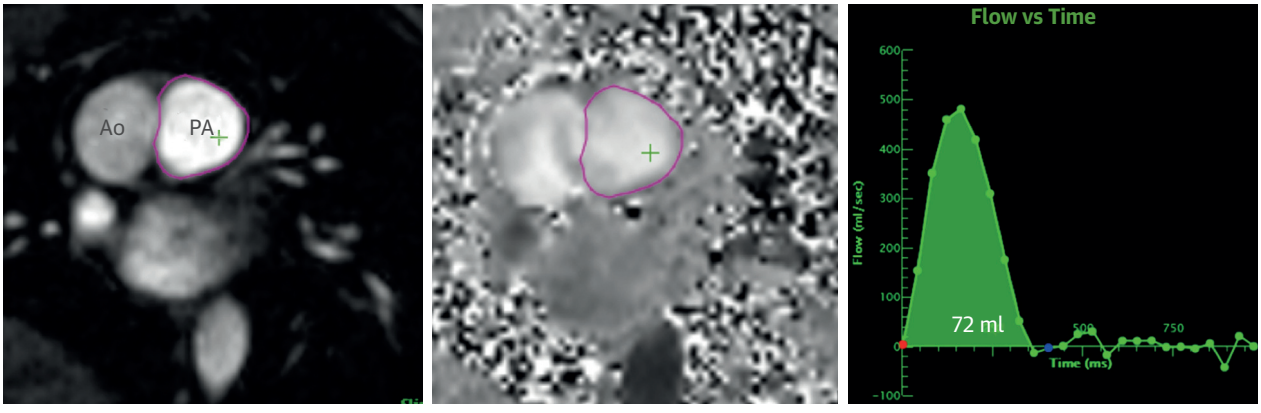

(Left) Anatomical cine image. **(Middle)** Velocity map measuring flow through the main pulmonary artery **(purple outline)**. **(Right)** Integral of flow-time curve to determine stroke volume using post-processing software. AO = Aorta; PA = pulmonary artery.

FIGURE 8 CMR Late Gadolinium Enhancement of the Right Ventricle

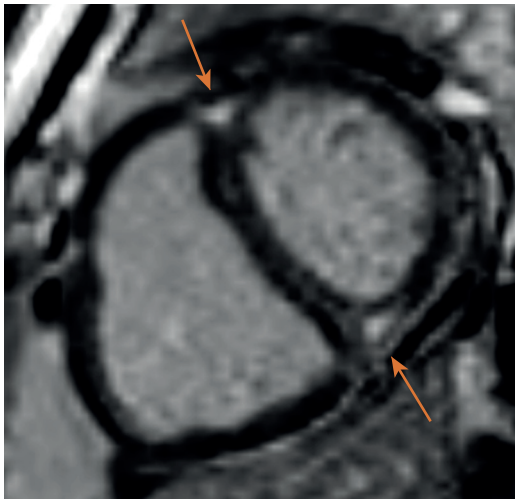

Bright areas **(orange arrows)** represent fibrosis of right ventricular insertion points into interventricular septum, typical of right ventricular pathologies. CMR = cardiac magnetic resonance image.

manually identified based on the smallest and largest volumes, respectively. In cases of dyssynchronous contraction, end-diastolic and end-systolic phases may vary between the LV and RV and should be individually traced. Trabeculations should be traced as part of the ventricular cavity (31). Stroke volume and EF can be mathematically determined from end-systolic and end-diastolic volumes. Normal RV volumes by CMR are endorsed by society guidelines (32). Normal reference ranges for RV volumes are higher in younger patients, males, and higher body surface areas (32).

Most studies have shown an underestimation of cardiac volumes by 2D and 3D echocardiography compared to CMR volumes (33–35). CMR short-axis stack volume tracings are accurate within 2% compared to ex-vivo animal and human heart volumes, using direct water displacement techniques as the gold standard (36,37). Some studies have advocated an additional stack of axial slices for quantification of RV volumes and EF (38,39). Although this approach was initially proposed to sidestep the difficulty in identifying the basal ventricular slice, it may no longer be necessary with the advent of colocalization features in most current post-processing software.

Similar to RV volumes, RV mass is calculated with the Simpson's method by tracing the epicardial and endocardial borders and excluding the papillary muscles. RV mass is reproducible with intraclass correlation values of >0.85 for intraobserver, interobserver, and interstudy variability (40). Normal reference ranges are published for RV mass, with higher masses observed in males, younger patients, and higher body surface areas (32).

Flow measurements use phase-contrast sequences which generate magnitude images and phase velocity maps (**Figure 7**). The magnitude image is used for anatomic orientation of the imaging slice and to identify the boundaries of the vessel imaged. The phase map encodes the velocities within each pixel for each phase in the cardiac cycle. A region of interest can be traced by using both of the images at each time point, and flow is quantified by integrating the velocity of each pixel and its area over the cardiac cycle. Unlike echocardiography, the imaging plane is prescribed perpendicularly to flow direction and does not make assumptions that the vessel cross-sectional area is constant throughout the cardiac cycle. CMR flow measurements have extensive validation in both in-vitro and in vivo studies (41–44).

Accurate and reliable measurements of ventricular volumes and function make CMR well suited to assess both the ventricular remodeling that is a consequence of TV pathology and the reverse remodeling that may occur with valvular interventions. In patients undergoing TV surgery for functional TR, studies by Choi et al. (45) and Kim et al. (46) demonstrated post-operative reductions in RV end-diastolic volume index (RVEDVi) and RV end-systolic index (RVESVi) measured by CMR. Kim et al. (46) found that, in patients with reduced RV systolic function, a pre-operative RVEDVi of <164 ml/m^2 was associated with a post-operative return to normal RV systolic function. Park et al. (47) showed incremental value of CMR RV volume and function measurements in patients with severe isolated TR requiring surgery who underwent both pre-operative echocardiography and CMR. After a mean post-operative follow-up of 57 months, the only parameters associated with cardiac death were CMR-quantified RVEF and RVESVi, with a hazard ratio of 0.7 per 5% increase in RVEF and 1.2 per 10 ml/m^2 increase in RVESVi (47).

RV REGIONAL WALL MOTION ASSESSMENT. Regional wall motion abnormalities are prevalent in the setting of myocardial infarction, pulmonary embolism, and PH. Owing to CMR's ability to dynamically visualize the RV in any imaging plane, this mode is ideal for assessment of regional RV wall motion abnormalities. Although a short-axis stack is used for assessment of volumes and function, a stack of long-

FIGURE 9 MDCT-Based Tricuspid Valve Apparatus Measurements

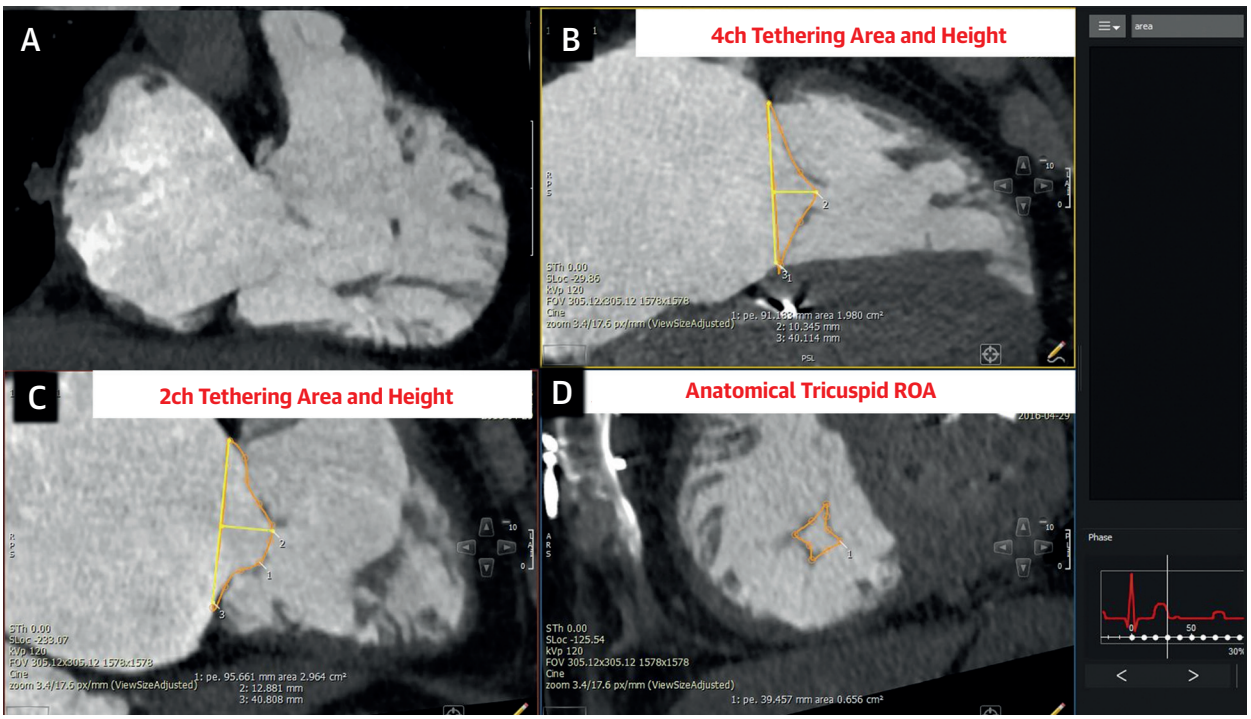

A multiplanar reconstruction of the tricuspid apparatus is shown. **(A)** Sagittal view of the right ventricle. **(B and C)** Measurements of tethering area and height, respectively. **(D)** Measurement of anatomical regurgitant orifice area that can be obtained by MDCT. MDCT = multidetector row computed tomography; ROA = regurgitant orifice area.

axis cines is recommended for assessment of regional RV wall motion abnormalities, especially for locations that are difficult to appreciate, such as the RVOT and RV free wall (48).

Feature tracking, similar in concept to speckle tracking in echocardiography, has been attempted to detect subtle changes in wall motion. Strain analysis is more sensitive than conventional measurements of RV wall motion and can predict future outcomes in specific cohorts of arrhythmogenic RV dysplasia and PH (49,50). However, this technology is still under investigation and is limited by poor interstudy and intervendor reproducibility (51,52).

TISSUE CHARACTERIZATION. Tissue characterization of the RV, using late gadolinium enhancement and native T1 imaging, is currently challenged by the spatial resolution of these imaging sequences for the thin-walled RV (29). Given the normal RV thickness of 3 to 5 mm, partial volume effects can create difficulty for nontransmural RV pathology (53). Alternatively, late gadolinium enhancement can be appreciated in transmural RV infarction and under conditions of increased RV wall thickness such as acute myocarditis, amyloidosis, and PH (54–57) (**Figure 8**). Similarly, native T1 assessment is possible under conditions of increased RV wall thickness, most notably in Anderson-Fabry disease and PH (58). Newer investigational techniques to improve the ability for accurate native T1 mapping include RV systolic imaging, when the wall is thicker, or high-resolution image acquisition using navigator-gated 3D techniques (59,60). Such techniques need further validation, and the latter technique would benefit from additional technological advances to decrease image acquisition times (59,60).

RA AND TV. Each long-axis view can visualize 2 of the 3 TV leaflets (**Figure 5**); however, only 1 leaflet can be reliably localized. If an abnormality is identified between 2 leaflets, a continuous stack of thin slices (4 to 5 mm) without an interslice gap, parallel to the leaflets in question, should be acquired to better delineate specific pathology (29). Leaflet tenting, restriction, prolapse, regurgitation, thickening, and perforation can be visualized with CMR. Cine images represent a consolidation of data acquired over several cardiac cycles, and therefore, objects with

FIGURE 10 MDCT Analysis of Tricuspid Valve Apparatus for Percutaneous Tricuspid Interventions

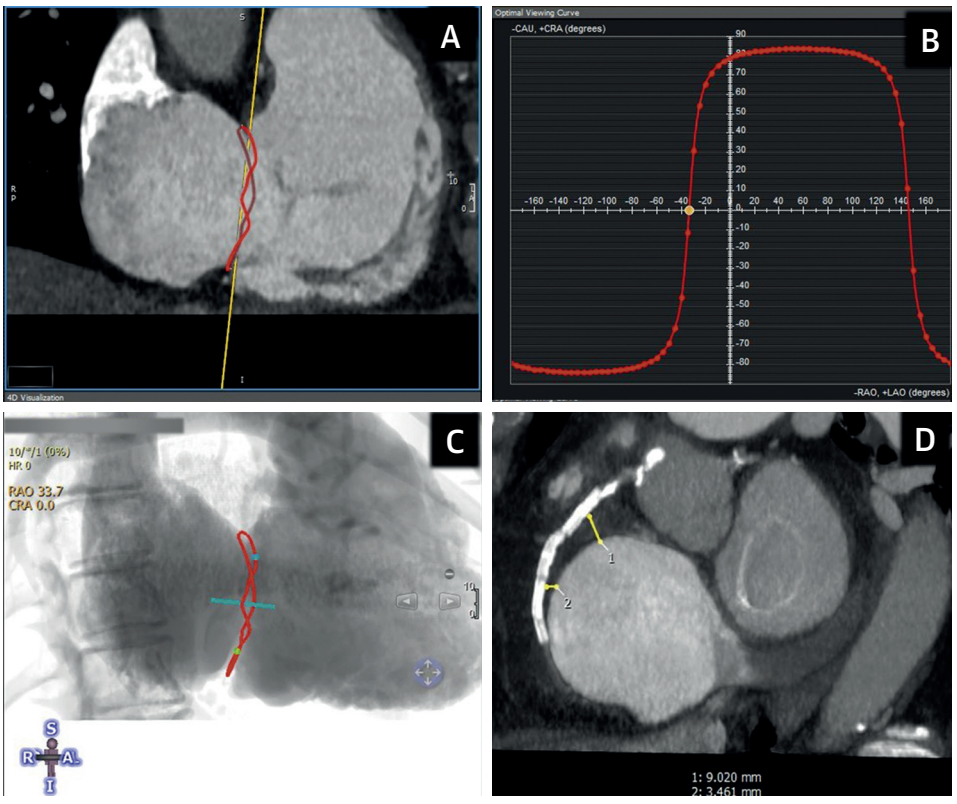

(A) Measurement of the tricuspid annulus using semiautomated cubic spline analysis. **(B)** Curve of coplanar angiographic projections for guidance of percutaneous tricuspid annulus interventions. **(C)** MDCT-derived angiographic simulation. **(D)** Location of the right coronary artery in relationship to the tricuspid annulus is shown. This may be relevant for percutaneous interventions affecting the tricuspid annulus, which could theoretically impinge upon the RCA. The RCA runs near the annulus in the right atrioventricular groove adjacent to the RV free wall. RCA = right coronary artery; other abbreviation as in Figure 9.

highly irregular or random motion may not be well visualized. This applies to torn chordae and small mobile masses.

The RA is generally visualized in 2 long-axis views: the standard 4-chamber and the specialized RV 3-chamber views. RA volumes can be estimated by using a single-plane area-length method in the 4-chamber view at ventricular end systole. Similar to RV volumes, normal RA volume reference ranges are higher in males, younger subjects, and those with larger body surface areas (61). A more extensive and reproducible assessment of volume can be calculated if a stack of short-axis images is acquired through the RA, at the expense of additional scan time (61).

CMR EVALUATION IN THE PRESENCE OF CARDIAC ARRHYTHMIA. It is important to note that patients with isolated TV or TV and MV disease often present with atrial dilation that predisposes them to atrial arrhythmia. In the presence of arrhythmia, accuracy of quantification of volumes and/or EF may be compromised. In the ideal scenario, multiple cardiac cycles should be averaged. Breath-held, segmented, steady-state free precession is the routine pulse sequence used in CMR for evaluation of systolic function in patients with normal sinus rhythm. However, use of CMR in patients with atrial fibrillation is associated with motion artifacts. One solution is real-time cine imaging with free breathing. This produces cine images similar to those in echocardiography, albeit with lower temporal and spatial resolution, given its short interval for acquisition. Technological advances in CMR with new pulse sequences and imaging reconstruction algorithms allow creation of real-time free-breathing cine images with

excellent quality and with superior spatial and temporal resolution compared to conventional breath-held, segmented acquisition (62,63).

For flow quantification in patients with cardiac arrhythmias, free-breathing phase-contrast acquisitions with an increased number of signal averages (minimum of 3) should provide an average of multiple cardiac cycles and allow quantification similar to breath-held acquisitions (64).

MDCT IMAGING OF THE TV AND RH

MDCT ACQUISITION OF THE RH. The complex and large anatomy of the TV makes MDCT acquisition challenging. Adequate opacification of the RH requires specific acquisition protocols. In order to avoid streak artifacts, a triphasic contrast bolus admixture (contrast, then contrast/saline, and then saline) protocol at a specific injection rate and total contrast volume should be used. Protocols that combine weight, LVEF, and heart rate have been suggested (65).

Equally important are the specifications of the MDCT scanner. Atrial fibrillation poses a challenge to older generation MDCT scanners, where a lower number of detector rows and lower temporal resolution may cause motion and misregistration artifacts (66). High temporal resolution (<80 to 100 ms) can be achieved by use of dual-source scanners or multi-segmented reconstruction algorithms for single-source scanners. In the latter protocol, the 180° data required is obtained from ≥2 consecutive heart beats. The tradeoff is longer scanning time, greater radiation dose, and contrast volume. Heart rate control is also needed to avoid motion and misregistration artifacts (66).

MDCT: FUNCTIONAL RIGHT-SIDED EVALUATION. Multiphasic, cardiac-gated acquisition encompassing the entire cardiac cycle is key to enabling data selection for image reconstruction from these patients, from the most stationary phase of the cardiac cycle. In addition, MDCT provides the opportunity to evaluate dynamic changes in systole and diastole and to evaluate RA and RV size, remodeling, and systolic function. Although the patient is exposed to increased radiation compared to conventional coronary protocols where only diastole is imaged, newer generation scanners with greater z-axis coverage have allowed for substantially shorter scan times, less iodinated contrast, and lower radiation dose.

Evaluation of cardiac function by MDCT angiography involves semiautomated segmentation of the ventricles, using at least 10 phases of cardiac cycle (5% to 95% of R-R interval) (67,68). High-spatial resolution images from MDCT provide excellent definition of the endocardial-blood pool interface. Studies comparing cardiac magnetic resonance imaging to MDCT functional assessment of RV volumes, RVEF, and stroke volumes have shown excellent correlations (69,70). MDCT is an important alternative in patients with certain implantable cardiac-defibrillators/resynchronization therapy devices which have not been considered safe for CMR scanning. Large, multicenter registry data have provided normal values for the RA and RV in healthy, normal control subjects free of hypertension and obesity (71).

MDCT FOR TR: ANATOMICAL CHANGES. In the context of TR, precise delineation of the right-sided anatomy and morphological changes can be clearly depicted by MDCT. Nemoto et al. (72) concluded that even patients with mild TR, compared to those with none or trace TR, demonstrated significant biatrial and tricuspid annular dilation. RV dilation is seen more commonly in those with severe TR and therefore could suggest a late phenomenon (72). Atrial fibrillation is a secondary insult which perpetuates the cycle of RA-TA enlargement that facilitates atrial fibrillation recurrence and begets more TR. Interestingly, TR, rather than PH, is a stronger driver of the remodeling changes seen by MDCT in the RA and TA for patients with a wide spectrum of TR severity (73).

MDCT is useful for the anatomical evaluation of the TA and the complex 3D anatomy of the RV and its components (**Figure 9A**). In addition, parameters such as TV leaflet tethering height, tethering area, and anatomical tricuspid regurgitant orifice area can be measured by MDCT (**Figures 9B to 9D**). Importantly, some of these parameters have been associated with recurrence of TR after surgical intervention (74,75). The utility of these parameters in the prediction of procedural success for transcatheter TV interventions (TTVI) will require further validation.

Retrograde contrast opacification of the inferior vena cava and/or hepatic veins on MDCT is a specific but not sensitive sign of RH disease (TR, PH, and/or RV systolic dysfunction) (76).

MDCT FOR TTVI. Several percutaneous methods have been developed for TTVI. These include coaptation/spacer devices (Forma, Edwards Lifesciences, Washington, DC), annular reduction (TriCinch, 4Tech Cardio Ltd., Galway, Ireland), Trialign (Mitralign, Inc., Tewksbury, Massachusetts), Millipede (Millipede, Inc., Santa Rosa, California), Cardioband (Edwards Lifesciences), edge-to-edge repair (MitraClip, Abbott, Abbott Park, Illinois), heterotopic caval valve implantation, and total transcatheter TV replacement

(Gate, Navigate Cardiac Structures Inc., Lake Forest, California) (77).

Comprehensive reviews of the specific imaging requirements for those TTVI therapies have been recently published (78–80). Given this rapidly evolving field, specific details of MDCT imaging analysis should therefore be reviewed by a heart team to ensure that the specific anatomical measurements of each of these therapeutic interventions is performed (79,80). TA sizing is important for plication and valve replacement. The distance between the right coronary artery and the TA is of potential importance for avoidance of coronary injury from annuloplasty devices (**Figure 10D**). Anatomical planning to achieve a perpendicular angle of the implant and avoid parallax can also be achieved with dedicated software (**Figures 10A to 10C**). Characterization of RV anatomy and trabeculations is critical for devices anchored in the endocardium. The role of MDCT for TTVI planning will continue to grow as percutaneous methods are established.

FLUOROSCOPIC RH ANATOMY

Standard views obtained on cross-sectional modalities such as echocardiography, CMR, and MDCT are possible fluoroscopically. Although these fluoroscopic views do not provide the details obtained from the aforementioned modalities, the need to correlate RH anatomical landmarks such as the RA, RV, interatrial septum, TA, IVC, coronary sinus, and right coronary artery fluoroscopically is gaining importance as tricuspid interventions are investigated. Generally, achievable fluoroscopic views can be used to simulate basal short-axis ("1-chamber") and 2-, 3-, and 4-chamber cross-sectional views of the RH and can be predicted by MDCT. Achievement of these views has been discussed extensively in a prior review (81).

CONCLUSIONS

Multimodality imaging is crucial in the complete evaluation of RH and TV anatomy. Its importance will continue to increase as the TV and RH are targeted for percutaneous transcatheter interventions.

ADDRESS FOR CORRESPONDENCE: Dr. Omar Khalique, Columbia University Medical Center, Department of Medicine, 5-501C, 177 Fort Washington Avenue, New York, New York 10032. E-mail: ok2203@cumc.columbia.edu. Twitter: @OKhaliqueMD

REFERENCES

1. Topilsky Y, Nkomo VT, Vatury O, et al. Clinical outcome of isolated tricuspid regurgitation. J Am Coll Cardiol Img 2014;7:1185–94.

2. Sorabella RA, Mamuyac E, Yerebakan H, et al. Residual tricuspid regurgitation following tricuspid valve repair during concomitant valve surgery worsens late survival. Heart Surg Forum 2015;18:E226–31.

3. King RM, Schaff HV, Danielson GK, et al. Surgery for tricuspid regurgitation late after mitral valve replacement. Circulation 1984;70:I193–7.

4. Ohno Y, Attizzani GF, Capodanno D, et al. Association of tricuspid regurgitation with clinical and echocardiographic outcomes after percutaneous mitral valve repair with the MitraClip System: 30-day and 12-month follow-up from the GRASP Registry. Eur Heart J Cardiovasc Imaging 2014;15:1246–55.

5. Barbanti M, Binder RK, Dvir D, et al. Prevalence and impact of preoperative moderate/severe tricuspid regurgitation on patients undergoing transcatheter aortic valve replacement. Catheter Cardiovasc Interv 2015;85:677–84.

6. Topilsky Y, Khanna A, Le Tourneau T, et al. Clinical context and mechanism of functional tricuspid regurgitation in patients with and without PH. Circ Cardiovasc Imaging 2012;5:314–23.

7. Hahn RT. State-of-the-Art review of echocardiographic imaging in the evaluation and treatment of functional tricuspid regurgitation. Circ Cardiovasc Imaging 2016;9. pii:e005332.

8. Muraru D, Surkova E, Badano LP. Revisit of functional tricuspid regurgitation; current trends in the diagnosis and management. Korean Circ J 2016;46:443–55.

9. Dahou ALD, Reisman M, Hahn RT. Gross anatomy of the tricuspid valve. J Am Coll Cardiol Img 2019.

10. Lancellotti P, Tribouilloy C, Hagendorff A, et al. Recommendations for the echocardiographic assessment of native valvular regurgitation: an executive summary from the European Association of Cardiovascular Imaging. Eur Heart J Cardiovasc Imaging 2013;14:611–44.

11. Muraru D, Hahn RT, Soliman OI, Faletra FF, Basso C, Badano LP. 3-dimensional echocardiography in imaging the tricuspid valve. J Am Coll Cardiol Img 2019;12:500–15.

12. Muraru D, Badano LP, Sarais C, Solda E, Iliceto S. Evaluation of tricuspid valve morphology and function by transthoracic three-dimensional echocardiography. Curr Cardiol Rep 2011;13:242–9.

13. Miglioranza MH, Mihaila S, Muraru D, Cucchini U, Iliceto S, Badano LP. Variability of tricuspid annulus diameter measurement in healthy volunteers. J Am Coll Cardiol Img 2015;8:864–6.

14. Dreyfus J, Durand-Viel G, Raffoul R, et al. Comparison of 2-dimensional, 3-dimensional, and surgical measurements of the tricuspid annulus size: clinical implications. Circ Cardiovasc Imaging 2015;8:e003241.

15. Ring L, Rana BS, Kydd A, Boyd J, Parker K, Rusk RA. Dynamics of the tricuspid valve annulus in normal and dilated RHs: a three-dimensional transoesophageal echocardiography study. Eur Heart J Cardiovasc Imaging 2012;13:756–62.

16. Maffessanti F, Gripari P, Pontone G, et al. Three-dimensional dynamic assessment of tricuspid and mitral annuli using cardiovascular magnetic resonance. Eur Heart J Cardiovasc Imaging 2013;14:986–95.

17. Anwar AM, Soliman OI, Nemes A, van Geuns RJ, Geleijnse ML, Ten Cate FJ. Value of assessment of tricuspid annulus: real-time three-dimensional echocardiography and magnetic resonance imaging. Int J Cardiovasc Imaging 2007;23:701–5.

18. Anwar AM, Geleijnse ML, Ten Cate FJ, Meijboom FJ. Assessment of tricuspid valve annulus size, shape and function using real-time three-dimensional echocardiography. Interact Cardiovasc Thorac Surg 2006;5:683–7.

19. van Rosendael PJ, Joyce E, Katsanos S, et al. Tricuspid valve remodelling in functional tricuspid regurgitation: multidetector row computed tomography insights. Eur Heart J Cardiovasc Imaging 2016;17:96–105.

20. Dreyfus GD, Martin RP, Chan KM, Dulguerov F, Alexandrescu C. Functional tricuspid regurgitation:

a need to revise our understanding. J Am Coll Cardiol 2015;65:2331–6.

21. Kim HK, Kim YJ, Park JS, et al. Determinants of the severity of functional tricuspid regurgitation. Am J Cardiol 2006;98:236–42.

22. Lang RM, Badano LP, Mor-Avi V, et al. Recommendations for cardiac chamber quantification by echocardiography in adults: an update from the American Society of Echocardiography and the European Association of Cardiovascular Imaging. Eur Heart J Cardiovasc Imaging 2015;16:233–70.

23. Muraru D, Spadotto V, Cecchetto A, et al. New speckle-tracking algorithm for right ventricular volume analysis from three-dimensional echocardiographic data sets: validation with cardiac magnetic resonance and comparison with the previous analysis tool. Eur Heart J Cardiovasc Imaging 2016;17:1279–89.

24. Addetia K, Maffessanti F, Muraru D, et al. Morphologic analysis of the normal right ventricle using three-dimensional echocardiography-derived curvature indices. J Am Soc Echocardiogr 2018;31:614–23.

25. Sugeng L, Mor-Avi V, Weinert L, et al. Multimodality comparison of quantitative volumetric analysis of the right ventricle. J Am Coll Cardiol Img 2010;3:10–8.

26. Galderisi M, Cosyns B, Edvardsen T, et al. Standardization of adult transthoracic echocardiography reporting in agreement with recent chamber quantification, diastolic function, and heart valve disease recommendations: an expert consensus document of the European Association of Cardiovascular Imaging. Eur Heart J Cardiovasc Imaging 2017;18:1301–10.

27. Peluso D, Badano LP, Muraru D, et al. Right atrial size and function assessed with three-dimensional and speckle-tracking echocardiography in 200 healthy volunteers. Eur Heart J Cardiovasc Imaging 2013;14:1106–14.

28. Carr JC, Simonetti O, Bundy J, Li D, Pereles S, Finn JP. Cine MR angiography of the heart with segmented true fast imaging with steady-state precession. Radiology 2001;219:828–34.

29. Kramer CM, Barkhausen J, Flamm SD, Kim RJ, Nagel E. Standardized cardiovascular magnetic resonance (CMR) protocols 2013 update. J Cardiovasc Magn Reson 2013;15:91.

30. Rudski LG, Lai WW, Afilalo J, et al. Guidelines for the echocardiographic assessment of the RH in adults: a report from the American Society of Echocardiography endorsed by the European Association of Echocardiography, a registered branch of the European Society of Cardiology, and the Canadian Society of Echocardiography. J Am Soc Echocardiogr 2010;23:685–713. quiz 786–8.

31. Schulz-Menger J, Bluemke DA, Bremerich J, et al. Standardized image interpretation and post processing in cardiovascular magnetic resonance: Society for Cardiovascular Magnetic Resonance (SCMR) board of trustees task force on standardized post processing. J Cardiovasc Magn Reson 2013;15:35.

32. Kawel-Boehm N, Maceira A, Valsangiacomo-Buechel ER, et al. Normal values for cardiovascular magnetic resonance in adults and children. J Cardiovasc Magn Reson 2015;17:29.

33. Caiani EG, Corsi C, Zamorano J, et al. Improved semiautomated quantification of left ventricular volumes and ejection fraction using 3-dimensional echocardiography with a full matrix-array transducer: comparison with magnetic resonance imaging. J Am Soc Echocardiogr 2005;18:779–88.

34. Mor-Avi V, Jenkins C, Kuhl HP, et al. Real-time 3-dimensional echocardiographic quantification of left ventricular volumes: multicenter study for validation with magnetic resonance imaging and investigation of sources of error. J Am Coll Cardiol Img 2008;1:413–23.

35. Tamborini G, Piazzese C, Lang RM, et al. Feasibility and accuracy of automated software for transthoracic three-dimensional left ventricular volume and function analysis: comparisons with two-dimensional echocardiography, three-dimensional transthoracic manual method, and cardiac magnetic resonance imaging. J Am Soc Echocardiogr 2017;30:1049–58.

36. Koch JA, Poll LW, Godehardt E, Korbmacher B, Modder U. Right and left ventricular volume measurements in an animal heart model in vitro: first experiences with cardiac MRI at 1.0 T. Eur Radiol 2000;10:455–8.

37. Jauhiainen T, Jarvinen VM, Hekali PE, Poutanen VP, Penttila A, Kupari M. MR gradient echo volumetric analysis of human cardiac casts: focus on the right ventricle. J Comput Assist Tomogr 1998;22:899–903.

38. Alfakih K, Plein S, Bloomer T, Jones T, Ridgway J, Sivananthan M. Comparison of right ventricular volume measurements between axial and short axis orientation using steady-state free precession magnetic resonance imaging. J Magn Reson Imaging 2003;18:25–32.

39. Clarke CJ, Gurka MJ, Norton PT, Kramer CM, Hoyer AW. Assessment of the accuracy and reproducibility of RV volume measurements by CMR in congenital heart disease. J Am Coll Cardiol Img 2012;5:28–37.

40. Catalano O, Antonaci S, Opasich C, et al. Intra-observer and interobserver reproducibility of right ventricle volumes, function and mass by cardiac magnetic resonance. J Cardiovasc Med (Hagerstown) 2007;8:807–14.

41. Sondergaard L, Lindvig K, Hildebrandt P, et al. Quantification of aortic regurgitation by magnetic resonance velocity mapping. Am Heart J 1993;125:1081–90.

42. Sondergaard L, Thomsen C, Stahlberg F, et al. Mitral and aortic valvular flow: quantification with MR phase mapping. J Magn Reson Imaging 1992;2:295–302.

43. Gatehouse PD, Rolf MP, Graves MJ, et al. Flow measurement by cardiovascular magnetic resonance: a multicentre multivendor study of background phase offset errors that can compromise the accuracy of derived regurgitant or shunt flow measurements. J Cardiovasc Magn Reson 2010;12:5.

44. Wilkoff BL, Bello D, Taborsky M, et al. Magnetic resonance imaging in patients with a pacemaker system designed for the magnetic resonance environment. Heart Rhythm 2011;8:65–73.

45. Choi JW, Park EA, Lee W, et al. Changes in right ventricular volume and function after tricuspid valve surgery- tricuspid annuloplasty vs. tricuspid valve replacement. Circ J 2016;80:1142–7.

46. Kim H-K, Kim Y-J, Park E-A, et al. Assessment of haemodynamic effects of surgical correction for severe functional tricuspid regurgitation: cardiac magnetic resonance imaging study. Eur Heart J 2010;31:1520–8.

47. Park JB, Kim HK, Jung JH, et al. Prognostic value of cardiac MR imaging for preoperative assessment of patients with severe functional tricuspid regurgitation. Radiology 2016;280:723–34.

48. te Riele AS, Tandri H, Bluemke DA. Arrhythmogenic right ventricular cardiomyopathy (ARVC): cardiovascular magnetic resonance update. J Cardiovasc Magn Reson 2014;16:50.

49. Heermann P, Hedderich DM, Paul M, et al. Biventricular myocardial strain analysis in patients with arrhythmogenic right ventricular cardiomyopathy (ARVC) using cardiovascular magnetic resonance feature tracking. J Cardiovasc Magn Reson 2014;16:75.

50. de Siqueira ME, Pozo E, Fernandes VR, et al. Characterization and clinical significance of right ventricular mechanics in PH evaluated with cardiovascular magnetic resonance feature tracking. J Cardiovasc Magn Reson 2016;18:39.

51. Morton G, Schuster A, Jogiya R, Kutty S, Beerbaum P, Nagel E. Inter-study reproducibility of cardiovascular magnetic resonance myocardial feature tracking. J Cardiovasc Magn Reson 2012;14:43.

52. Gertz RJ, Lange T, Kowallick JT, et al. Inter-vendor reproducibility of left and right ventricular cardiovascular magnetic resonance myocardial feature-tracking. PloS One 2018;13:e0193746.

53. Grosse-Wortmann L, Macgowan CK, Vidarsson L, Yoo SJ. Late Gadolinium Enhancement of the right ventricular myocardium: is it really different from the left? J Cardiovasc Magn Reson 2008;10:20.

54. Freed BH, Collins JD, Francois CJ, et al. MR and CT Imaging for the evaluation of PH. J Am Coll Cardiol Img 2016;9:715–32.

55. Grothoff M, Elpert C, Hoffmann J, et al. Right ventricular injury in ST-elevation myocardial infarction: risk stratification by visualization of wall motion, edema, and delayed-enhancement cardiac magnetic resonance. Circ Cardiovasc Imaging 2012;5:60–8.

56. Hama Y, Funabashi N, Ueda M, et al. Images in cardiovascular medicine. Right-sided heart wall thickening and delayed enhancement caused by chronic active myocarditis complicated by sustained monomorphic ventricular tachycardia. Circulation 2009;119:e200–3.

57. Maceira AM, Joshi J, Prasad SK, et al. Cardiovascular magnetic resonance in cardiac amyloidosis. Circulation 2005;111:186–93.

58. Pagano JJ, Chow K, Khan A, et al. Reduced right ventricular native myocardial t1 in anderson-fabry disease: comparison to PH and healthy controls. PLoS One 2016;11:e0157565.

59. Kawel-Boehm N, Dellas Buser T, Greiser A, Bieri O, Bremerich J, Santini F. In-vivo assessment of normal T1 values of the right-ventricular myocardium by cardiac MRI. Int J Cardiovasc Imaging 2014;30:323–8.

60. Nordio G, Henningsson M, Chiribiri A, Villa ADM, Schneider T, Botnar RM. 3D myocardial T1 mapping using saturation recovery. J Magn Reson Imaging 2017;46:218–27.

61. Sievers B, Addo M, Breuckmann F, Barkhausen J, Erbel R. Reference right atrial function determined by steady-state free precession cardiovascular magnetic resonance. J Cardiovasc Magn Reson 2007;9:807–14.

62. Xue H, Kellman P, Larocca G, Arai AE, Hansen MS. High spatial and temporal resolution retrospective cine cardiovascular magnetic resonance from shortened free breathing real-time acquisitions. J Cardiovasc Magn Reson 2013;15:102.

63. Axel L, Otazo R. Accelerated MRI for the assessment of cardiac function. Br J Radiol 2016; 89:20150655.

64. Cavalcante JL, Lalude OO, Schoenhagen P, Lerakis S. Cardiovascular magnetic resonance imaging for structural and valvular heart disease interventions. J Am Coll Cadiol Intv 2016;9: 399–425.

65. Hinzpeter R, Eberhard M, Burghard P, et al. Computed tomography in patients with tricuspid regurgitation prior to transcatheter valve repair: dynamic analysis of the annulus with an individually tailored contrast media protocol. EuroIntervention 2017;12:e1828–36.

66. Lewis MA, Pascoal A, Keevil SF, Lewis CA. Selecting a CT scanner for cardiac imaging: the heart of the matter. Br J Radiol 2016;89: 20160376.

67. Henneman MM, Schuijf JD, Jukema JW, et al. Assessment of global and regional left ventricular function and volumes with 64-slice MSCT: a comparison with 2D echocardiography. J Nucl Cardiol 2006;13:480–7.

68. Greupner J, Zimmermann E, Grohmann A, et al. Head-to-head comparison of left ventricular function assessment with 64-row computed tomography, biplane left cineventriculography, and both 2- and 3-dimensional transthoracic echocardiography: comparison with magnetic resonance imaging as the reference standard. J Am Coll Cardiol 2012;59:1897–907.

69. Plumhans C, Muhlenbruch G, Rapaee A, et al. Assessment of global right ventricular function on 64-MDCT compared with MRI. AJR Am J Roentgenol 2008;190:1358–61.

70. Maffei E, Messalli G, Martini C, et al. Left and right ventricle assessment with Cardiac CT: validation study vs. Cardiac MR. Eur Radiol 2012;22: 1041–9.

71. Lin FY, Devereux RB, Roman MJ, et al. Cardiac chamber volumes, function, and mass as determined by 64-multidetector row computed tomography: mean values among healthy adults free of hypertension and obesity. J Am Coll Cardiol Img 2008;1:782–6.

72. Nemoto N, Lesser JR, Pedersen WR, et al. Pathogenic structural heart changes in early tricuspid regurgitation. J Thorac Cardiovasc Surg 2015;150:323–30.

73. Nemoto N, Schwartz JG, Lesser JR, et al. The right atrium and tricuspid annulus are cardinal structures in tricuspid regurgitation with or without PH. In J Cardiol 2017;230:171–4.

74. Kabasawa M, Kohno H, Ishizaka T, et al. Assessment of functional tricuspid regurgitation using 320-detector-row multislice computed tomography: risk factor analysis for recurrent regurgitation after tricuspid annuloplasty. J Thorac Cardiovasc Surg 2014;147:312–20.

75. Fukuda S, Song JM, Gillinov AM, et al. Tricuspid valve tethering predicts residual tricuspid regurgitation after tricuspid annuloplasty. Circulation 2005;111:975–9.

76. Yeh BM, Kurzman P, Foster E, Qayyum A, Joe B, Coakley F. Clinical relevance of retrograde inferior vena cava or hepatic vein opacification during contrast-enhanced CT. AJR Am J Roentgenol 2004;183:1227–32.

77. Rodes-Cabau J, Hahn RT, Latib A, et al. Transcatheter therapies for treating tricuspid regurgitation. J Am Coll Cardiol 2016;67: 1829–45.

78. van Rosendael PJ, Kamperidis V, Kong WK, et al. Computed tomography for planning transcatheter tricuspid valve therapy. Eur Heart J 2017; 38:665–74.

79. Prihadi EA, Delgado V, Hahn RT, Leipsic J, Min JK, Bax JJ. Imaging needs in novel transcatheter tricuspid valve interventions. J Am Coll Cardiol Img 2018;11:736–54.

80. Naoum C, Blanke P, Cavalcante JL, Leipsic J. Cardiac computed tomography and magnetic resonance imaging in the evaluation of mitral and tricuspid valve disease: implications for transcatheter interventions. Circ Cardiovasc Imaging 2017;10. pii:e005331.

81. Pighi M, Theriault-Lauzier P, Alosaimi H, et al. Fluoroscopic anatomy of right-sided heart structures for transcatheter interventions. J Am Coll Cadiol Intv 2018;11:1614–25.

82. Lang RM, Badano LP, Mor-Avi V, et al. Recommendations for cardiac chamber quantification by echocardiography in adults: an update from the American Society of Echocardiography and the European Association of Cardiovascular Imaging. J Am Soc Echocardiogr 2015;28:1–39.

83. Stojanovska J, Prasitdumrong H, Patel S, et al. Reference absolute and indexed values for left and right ventricular volume, function and mass from cardiac computed tomography. J Med Imaging Radiat Oncol 2014;58: 547–58.

KEY WORDS multimodality imaging, tricuspid interventions, tricuspid valve